Available online at www.sciencedirect.com
ScienceDirect
Journal of the European Ceramic Society 30 (2010) 435–440
www.elsevier.com/locate/jeurceramsoc

Characterization of alkaline earth metals ruthenate thin films

Akihiko Ito [a,*], Hiroshi Masumoto [b], Takashi Goto [c], Shunichi Sato [a]

[a] *Institute of Multidisciplinary Research for Advanced Materials, Tohoku University, Sendai 980-8577, Japan*
[b] *Center for Interdisciplinary Research, Tohoku University, Sendai 980-8578, Japan*
[c] *Institute for Materials Research, Tohoku University, Sendai 980-8577, Japan*

Abstract

$SrRuO_3$ (SRO), $BaRuO_3$ (BRO) and $CaRuO_3$ (CRO) thin films prepared by laser ablation in a wide range of deposition conditions were investigated on the relationship between deposition conditions, phase formation, microstructure and electrical conductivity. The optimum conditions for preparing highly conductive thin films were investigated. SRO, CRO and BRO thin films were crystallized with pseudo-cubic SRO and CRO, and a 9R-type hexagonal BRO structure, respectively. SRO and BRO thin films were crystallized with fine grains, whereas rectangular-shaped island grains tended to grow on the CRO thin films. The electrical conductivity of SRO and BRO thin films increased with an increase in deposition temperature of substrate and an increase in oxygen pressure, meanwhile, in CRO thin films, only the CRO thin film with a continuous surface of connected grains exhibited metallic conduction. However, the electron conduction transition from semi-conducting behavior to metallic conduction occurred when σ of 10^4 S m^{-1} was reached independent of alkaline earth metal and microstructure. The optimum conditions were $T_{sub} = 773$ to 973 K and $P_{O_2} = 0.13$ to 13 Pa.

Keywords: Films; Electrical conductivity; Ruthenate

1. Introduction

The alkaline earth metals ruthenate $ARuO_3$ (A = Sr, Ba and Ca) are promising materials as conductive pastes and electrodes for microdevices because of their excellent electrical conductivity and chemical stability.[1,2] $SrRuO_3$ (SRO) and $CaRuO_3$ (CRO) have a slightly distorted $GdFeO_3$-type orthorhombic structure (*Pnma*; SRO: $a = 0.553$ nm, $b = 0.875$ nm and $c = 0.557$ nm, and CRO: $a = 0.536$ nm, $b = 0.766$ nm and $c = 0.553$ nm) that can be simplified as a pseudo-cubic perovskite structure, which basically consists of corner-sharing RuO_6 octahedra.[1,3] On the other hand, due to the large ionic radius of Ba, a pseudo-cubic structure with corner-sharing RuO_6 octahedra with face sharing is possible. Thus, there are various hexagonal poly-types of BRO depending on the number of periodically stacked RuO_6 octahedra. Nine-layered BRO (9R BRO; $R\bar{3}m$: $a = 0.575$ nm and $c = 2.161$ nm), in which the Ru_3O_{12} trimers of the face-sharing RuO_6 octahedra are joined by corner-sharing, is the most common structure,[3,4] whereas four- and six-layered BRO (4H BRO and 6H BRO; $P6_3/mmc$; 4H BRO: $a = 0.574$ nm and $c = 0.950$ nm, and 6H BRO: $a = 0.574$ nm and $c = 1.405$ nm), in which the Ru_2O_9 dimers of the face-sharing RuO_6 are joined by corner-sharing, are obtained as a high-pressure phase product.[5,6]

SRO thin film has been widely employed as electrodes for the ferroelectric oxide layer in microdevices due to its good performance,[2,7,8] although a magnetic phase transition restricts its application to magnetic devices operating at low temperatures. In that respect, CRO is paramagnetic independent of temperature, and therefore attractive for use in for magnetic devices such as Josephson devices.[9] BRO thin films have received relatively little attention even though BRO exhibits characteristic electrical properties different from those of CRO and SRO owing to the small Ru–Ru distance in the face-sharing RuO_6 octahedra.[10,11]

Epitaxial $ARuO_3$ thin films on single-crystal substrates such as $SrTiO_3$[1,12,13] and $LaAlO_3$[14,15] have been widely investigated. However, there has been no overall report on the relationship between deposition conditions, microstructure and electrical conductivity of polycrystalline $ARuO_3$ thin films. Due to the constrained conditions of epitaxial growth, the intrinsic nature and the role of the alkaline earth metal elements of $ARuO_3$ thin films has not been well elucidated. The present authors have previously reported on the preparation of each polycrystalline SRO, BRO and CRO thin films prepared on quartz glass substrates

* Corresponding author. Tel: +81 22 215 2106; fax: +81 22 215 2107.
E-mail address: itonium@imr.tohoku.ac.jp (A. Ito).

0955-2219/$ – see front matter © 2009 Elsevier Ltd. All rights reserved.
doi:10.1016/j.jeurceramsoc.2009.06.011

by laser ablation.[16–18] Laser ablation has been advantageous to prepare and compare the ruthenate films in a wide range of deposition conditions by comparison with the other vapor deposition methods such as sputtering or chemical vapor deposition.

In this paper, the effects of deposition conditions on the phase formation, microstructure and electrical conductivity of SRO, BRO and CRO thin films prepared by laser ablation were investigated and contrasted comprehensively. The optimum conditions for preparing a highly conductive thin film were proposed.

2. Experimental procedure

RuO_2 (99.99% purity, Furuya Metal Co. Ltd.), $SrCO_3$ (99.9% purity, Wako Pure Chemical Industries Ltd.), $BaCO_3$ (99.9% purity, Wako Pure Chemical Industries Ltd.) and $CaCO_3$ (99.99% purity, Wako Pure Chemical Industries Ltd.) powders were used for preparation of laser ablation targets. These powders were weighed, mixed, pressed into pellets and reacted at 1273 K for up to 86.4 ks to obtain SRO, BRO and CRO pellets. The SRO and BRO pellets were crushed and sintered again at 1573 K for 43.2 ks, thus obtaining SRO and BRO targets. To obtain CRO targets, CRO pellets were crushed and sintered by spark plasma sintering (SPS) at 80 MPa and 1373 K for 300 s.

A third harmonic wavelength of a Q-switch pulsed Nd:YAG (Spectron Laser System SL805, $\lambda = 355$ nm) was used for the ablation. The details of the experimental setup have been reported elsewhere.[16–18] Quartz glass plates (10 mm × 12 mm × 0.5 mm) were used as substrates. Depositions were carried out in a high vacuum ($P = 10^{-6}$ Pa) and in O_2 at oxygen pressures (P_{O_2}) from 0.013 to 130 Pa for deposition times (t_{dep}) of 3.6 and 7.2 ks. The substrate temperature (T_{sub}) was changed from room temperature to 1073 K.

The crystal phase was studied by X-ray diffraction (XRD, Rigaku RAD-2C). The binding energy was determined by X-ray photoelectron spectroscopy (XPS, Surface Science SX100). Surface morphology was observed by a field-emission scanning electron microscope (FESEM, JEOL JSM-6500FT). The composition was examined by energy dispersive X-ray spectroscopy (EDS) attached to FESEM. The electrical conductivity (σ) was measured from 60 to 723 K by the van der Pauw method.

3. Results and discussion

3.1. Phase formation

Figs. 1–3 show the phase formation diagrams of SRO, BRO and CRO thin films prepared at various T_{sub} and P_{O_2}. The details of the XRD and XPS results have been reported elsewhere.[16–18] Pseudo-cubic SRO thin films with a (1 1 0)-orientation were obtained at $T_{sub} > 773$ K and $P_{O_2} = 13$ *Pa* (filled circles in Fig. 1), whereas amorphous SRO thin films were formed at $T_{sub} < 573$ K and $P_{O_2} = 13$ *Pa* (×-indications in Fig. 1). SRO thin films were amorphous in a high vacuum and at $P_{O_2} = 0.13$ *Pa* independently of T_{sub}. The co-existence of free metallic Ru and SrO phase in the SRO thin films was identified by XPS studies for the thin films prepared in a high vacuum and

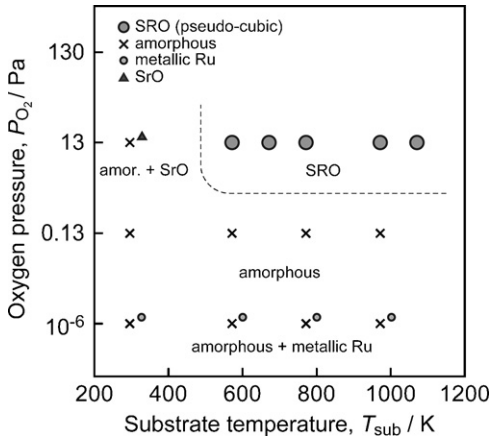

Fig. 1. Phase formation diagram of SRO thin films as functions of T_{sub} and P_{O_2} for $t_{dep} = 3.6$ ks.

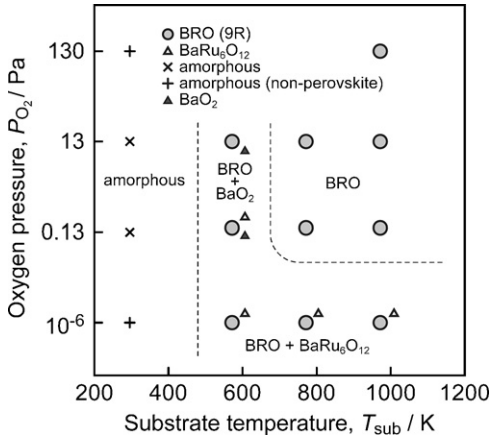

Fig. 2. Phase formation diagram of BRO thin films as functions of T_{sub} and P_{O_2} for $t_{dep} = 3.6$ ks.

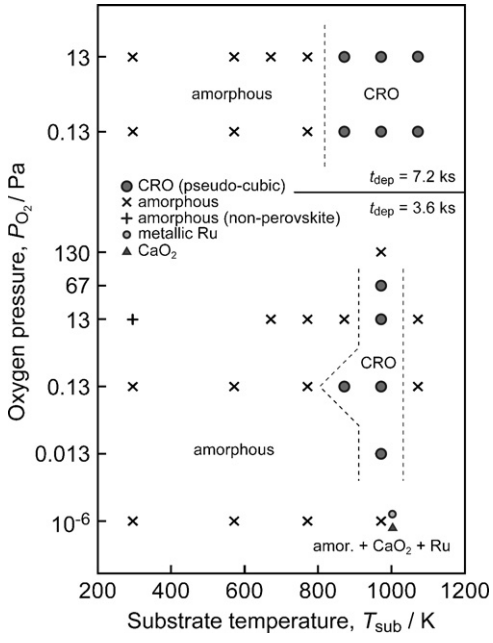

Fig. 3. Phase formation diagram of CRO thin films as functions of T_{sub} and P_{O_2} for $t_{dep} = 3.6$ and 7.2 ks.

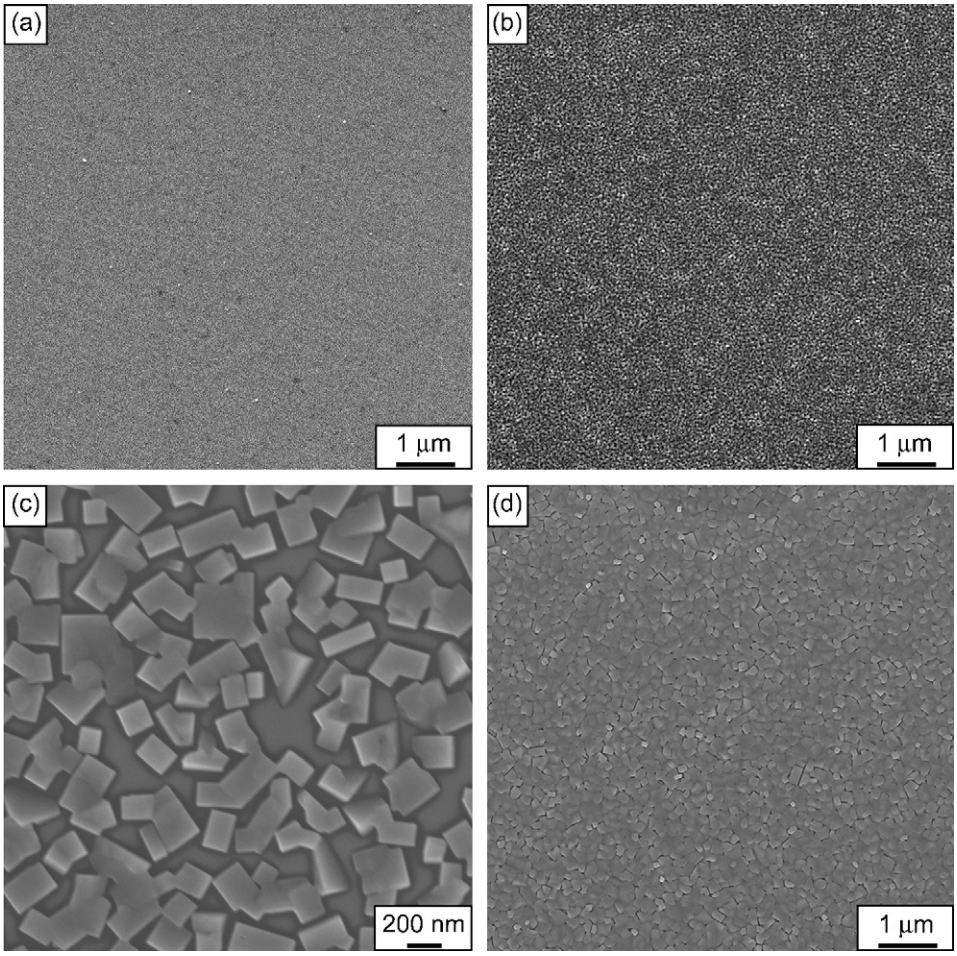

Fig. 4. FESEM images of SRO thin films prepared at $P_{O_2} = 13$ *Pa*, $T_{sub} = 773$ K (a), and $T_{sub} = 973$ K (b) for $t_{dep} = 3.6$ ks, and CRO thin films prepared at $P_{O_2} = 0.013$ *Pa* and $T_{sub} = 973$ K for $t_{dep} = 3.6$ ks (c), $P_{O_2} = 13$ *Pa*, and $P_{O_2} = 0.13$ *Pa* and $T_{sub} = 973$ K for $t_{dep} = 7.2$ ks (d).

at low T_{sub} (small circles and filled triangle in Fig. 1, respectively).

9R-type BRO thin films were obtained at $P_{O_2} > 0.13$ *Pa* and $T_{sub} > 573$ K (filled circles in Fig. 2). $BaRu_6O_{12}$ was formed as a second phase at $P = 10^{-6}$ Pa and $T_{sub} > 573$ K, and $P_{O_2} = 0.13$ *Pa* and $T_{sub} = 573$ K (open triangles in Fig. 2). BRO thin films prepared at $T_{sub} = 298$ K were amorphous independently of P_{O_2} (×-indicators in Fig. 2). As in the case of SRO, the alkaline earth oxide phase of BaO_2 in the BRO thin films were identified by XPS studies for the thin films prepared at $P_{O_2} = 0.13$ to 13 Pa and $T_{sub} = 573$ K (filled triangles in Fig. 2). The O 1s and Ba 3d XPS spectra of BRO thin films prepared at $T_{sub} = 298$ K and $P_{O_2} = 130$ *Pa* implied that the chemical bonds in the BRO thin films were different from those of the perovskite structure (cross marks in Fig. 2).

Pseudo-cubic CRO thin films were obtained at $T_{sub} = 973$ K and $P_{O_2} = 0.013$ to 67 Pa, and $T_{sub} = 873$ K and $P_{O_2} = 0.13$ *Pa* in the case of $t_{dep} = 3.6$ ks, and $T_{sub} > 873$ K and $P_{O_2} = 0.13$ and 130 Pa in the case of $t_{dep} = 7.2$ ks (filled circles in Fig. 3). At $T_{sub} < 773$ K, CRO thin films were amorphous independently of P_{O_2} and t_{dep} (× and cross marks in Fig. 3). Amorphous CRO thin films with the free metallic Ru and CaO_2 phase and were formed at $T_{sub} = 973$ K, $P = 10^{-6}$ Pa and $t_{dep} = 3.6$ ks (×-indications with a small circle and triangle in Fig. 3).

3.2. Microstructure

Fig. 4 shows the typical surface images of SRO, BRO and CRO thin films.[16–18] Amorphous-like SRO thin films prepared at $P = 10^{-6}$ Pa and $T_{sub} < 773$ K showed a flat, heterogeneous morphology (Fig. 4(a)). SRO thin films were crystallized as fine grains several tens of nanometers in size at $P_{O_2} > 0.13$ Pa and $T_{sub} > 773$ K (Fig. 4(b)), but then a coarse-grained surface was formed at higher T_{sub} and P_{O_2}, *i.e.*, $T_{sub} = 1073$ K and $P_{O_2} = 13$ *Pa* and $T_{sub} = 973$ K and $P_{O_2} = 67$ *Pa*. BRO thin films prepared in a low T_{sub} and P_{O_2} region were amorphous or had a secondary phases of BaO_2 showed a non-uniform texture, whereas BRO thin films obtained at $T_{sub} > 773$ K and $P_{O_2} = 13$ *Pa* consisted of slightly elongated fine grains several tens of nanometers in size as shown in Fig. 4(b) and CRO thin films prepared at $T_{sub} = 973$ K and $P = 10^{-6}$ Pa consisted of fine grains; however, rectangular-shaped island grains grew on the CRO thin films with the introduction of oxygen gas of $P_{O_2} > 0.013$ *Pa* (Fig. 4(c)). XRD results implied that the facet of the rectangular-shaped island grains would be the pseudo-cubic (1 0 0) CRO plane. The island grains showed a stoichiometric composition independent of T_{sub}, whereas the Ca fraction of the matrix increased with increasing T_{sub}. On the other hand, a flat, smooth morphology was observed at $T_{sub} < 573$ K and

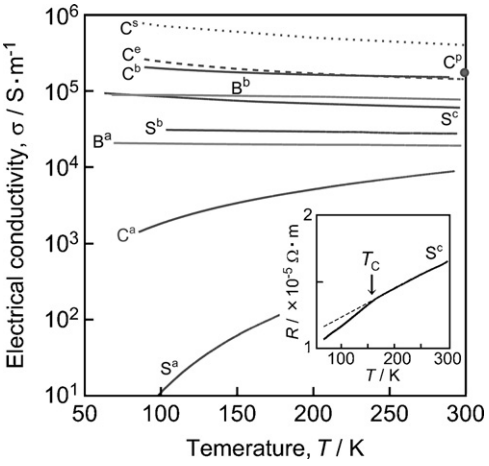

Fig. 5. Temperature dependence of electrical conductivity at low temperatures for SRO thin films prepared at $P_{O_2} = 13$ *pa* and $T_{sub} = 573$ K (S^a), 673 K (S^b) and 973 K (S^c), BRO thin films prepared at $P_{O_2} = 13$ *Pa* and $T_{sub} = 573$ K (B^a) and 773 K (B^b), CRO thin films prepared at $P_{O_2} = 0.13$ *Pa* and $T_{sub} = 873$ K (C^a) and 973 K (C^b) for $t_{dep} = 7.2$ ks, and the literature data of CRO: epitaxial thin film (C^e), polycrystalline sintered body (C^p) and single crystal (C^s). Inset shows the temperature dependence of electrical resistivity (R) around the Curie temperature (T_C) of the sample S^C.

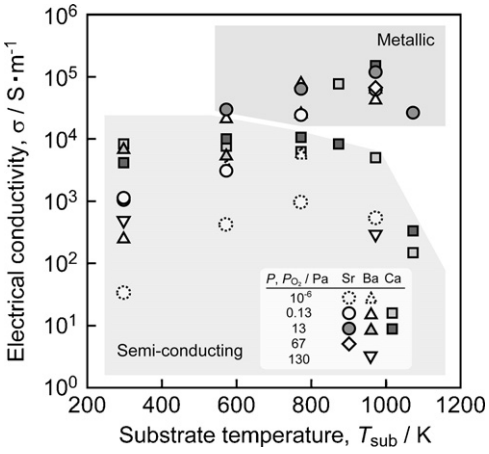

Fig. 6. Effect of T_{sub} and P_{O_2} on the σ of SRO (circles and diamond), BRO (triangles) and CRO (squares) thin films prepared at various P_{O_2}.

$P_{O_2} = 13$ Pa. With increasing T_{sub} from 573 to 973 K, the size and distribution density of the rectangular-shaped island grains increased. At higher T_{sub} of 1073 K, the edges of island grains were only rounded off, were not connected with each other. In the case of $t_{dep} = 7.2$ ks and $P_{O_2} = 0.13$ to 13 Pa, pseudo-cubic CRO thin films with rectangular-shaped island grains were obtained at $T_{sub} > 873$ K, whereas amorphous CRO thin films were formed at $T_{sub} < 773$ K. CRO thin films with the densely connected grains were obtained only at $T_{sub} = 973$ K and $P_{O_2} = 0.13$ *Pa*, and $T_{sub} = 873$ K and $P_{O_2} = 13$ *Pa* (Fig. 4(d)).

3.3. Electrical properties

Fig. 5 shows the representative temperature dependence of σ for SRO, BRO and CRO thin films prepared at various T_{sub} and P_{O_2}.[16–18] SRO thin films prepared at $P_{O_2} = 13$ *Pa* and $T_{sub} < 573$ K showed semi-conducting behavior, *i.e.*, the σ increased with increasing temperature (Fig. 5(S^a)). With increasing T_{sub}, the σ increased, changing the electron conduction from semi-conducting behavior to metallic conduction, *i.e.*, the σ decreased with increasing temperature (Fig. 5(S^b) and (S^c)). For SRO thin films prepared at $P_{O_2} = 13$ *Pa* and $T_{sub} = 773$ and 973 K, the temperature gradient of electrical resistivity changed at the Curie temperature of $T_C = 163$ K (Fig. 5, inset), implying a magnetic phase transition from paramagnetic to ferromagnetic. BRO thin films showed a tendency similar that of SRO thin films, and BRO thin films prepared at $T_{sub} > 573$ K showed metallic conduction (Fig. 5(B^a) and (B^b)). CRO thin films prepared at $t_{dep} = 3.6$ ks had a semi-conducting behavior independent of T_{sub} and P_{O_2}, whereas the CRO thin films prepared at $P_{O_2} = 0.13$ *Pa* and $T_{sub} = 973$ K (Fig. 5(C^b)) exhibited metallic conduction with high σ almost the same as that of the polycrystalline sintered body (Fig. 5(C^p))[19] and epitaxial thin film (Fig. 5(C^e)).[20]

Fig. 6 depicts the effect of T_{sub} on the σ of SRO, BRO and CRO thin films prepared at various P_{O_2}. The σ tended to increase with increasing T_{sub} and P_{O_2}, *i.e.*, $T_{sub} = 773$ to 973 K and $P_{O_2} = 0.13$ to 13 Pa, respectively, but then the σ decreased at higher T_{sub} and P_{O_2}. The electron conduction transition from semi-conducting behavior to metallic conduction occurred when σ of 10^4 S m^{-1} was reached independent of alkaline earth metal and microstructure. This transition at same regions ranging from 10^3 to 10^4 S m^{-1} have been reported in cases of the epitaxial SRO and CRO thin films which had Ru deficiency,[21] lattice strain[22,23] and disordered-structure.[24] Since the p–d hybridized orbital in RuO_6 octahedra, namely the strong correlation between Ru 4d t_{2g} and O 2p states, might play a significant role in the electrical conduction of $ARuO_3$, the structural disorder reduced the interactions between Ru and O orbital in RuO_6 octahedra, resulting in the decrease of σ and electron conduction transition.[25]

3.4. Optimum deposition conditions

Fig. 7 summarizes the effect of the deposition conditions on the microstructure and electrical properties. In low T_{sub} and P_{O_2} regions, the SRO and BRO thin films were amorphous and showed a low σ with semi-conducting behavior. The alkaline-earth metal oxide phases, SrO and BaO_2 were identified in a portion of those thin films at low T_{sub} and relatively high P_{O_2}. At $P = 10^{-6}$ Pa, the co-existence of the free metallic Ru and $BaRu_6O_{12}$ phase were observed for SRO and BRO, respectively. In the case of CRO, separated rectangular-shaped island grains tended to grow on the thin films, inhibiting metallic conduction of those thin films.

In general, the crystal structure and phase stability of perovskite ABO_3 can be estimated by the tolerance factor (t), namely the ratio between the radii of A- and B-site ions, and oxygen ion.[26] SRO with $t = 0.95$ has a nearly ideal perovskite structure such as $SrTiO_3$ ($t = 1.0$). BRO with $t = 1.1$ shows the perovskite-related structure due to the large ionic radius of Ba atom that leads a corner-sharing or face-sharing of Ru octahedral. This large ionic radius might allow a Ru-rich phase

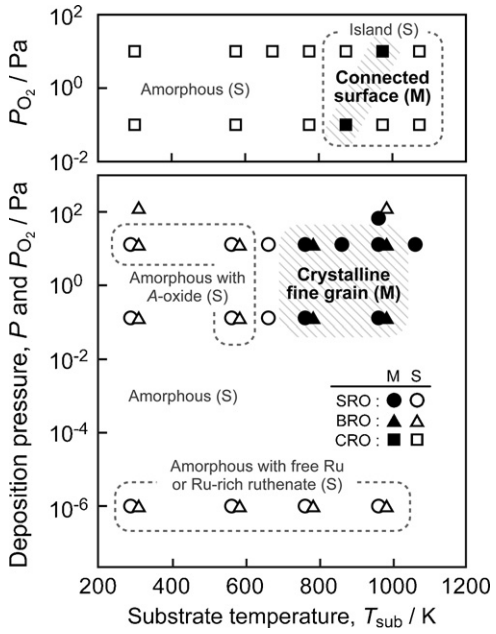

Fig. 7. Effect of T_{sub} and P_{O_2} on the microstructure and electron conduction of SRO (circles), BRO (triangles) and CRO (squares) thin films prepared at various conditions. Filled and open marks indicate metallic conduction (M) and semi-conducting behavior (S), respectively.

$BaRu_6O_{12}$ formation rather than the metallic Ru precipitation. For CRO with $t = 0.88$, the small ionic radius of Ca atom causes the lowering of symmetry in perovskite due to tilting of the octahedral and reduces the size of the oxygen sublattice. Thus the small radius of Ca atom might lead a rectangular-shaped island growth which reflects the oxygen sublattice. We have figured out that the $CaTiO_3$ (CTO) thin films prepared by laser ablation onto the metallic Ti substrate grew as the island grains and Yang et al. has also been reported that rectangular-shaped island growth of CTO on quartz glass substrate by laser ablation.[27] Although Ca-perovskite films prepared by laser ablation seems to tend to grow as the rectangular-shaped island, the present authors have recently reported that the addition of Ba to CRO was effective to prevent the growth of rectangular-shaped island grains.[28]

With increasing T_{sub} and P_{O_2}, the thin films crystallized into fine grains and the σ increased. At higher T_{sub} and P_{O_2}, the σ tended to decrease due to coarse-grains and non-stoichiometric composition. The thin films prepared at higher T_{sub} and P_{O_2}, which had high crystallinity and structural order without deficiency, would be highly conductive with metallic conduction. The continuous surface of CRO thin films with densely connected grains exhibited metallic conduction with excellent σ. The optimum conditions to prepare $ARuO_3$ thin films with higher σ were $T_{sub} = 773$ to 973 K and $P_{O_2} = 0.13$ to 13 Pa.

4. Conclusions

SRO, BRO and CRO thin films were prepared in a wide range of deposition conditions by laser ablation, and the optimum conditions for preparing a highly conductive thin film were investigated. Non-stoichiometric composition, structural disorder and co-existence of metallic Ru and mono-oxide reduced an electrical conductivity, causing semi-conducting behavior. High crystallinity and low oxygen deficiency led to the higher electrical conductivity with metallic conduction of the $ARuO_3$ thin films. Rectangular-shaped island grains grew on the CRO thin films, inhibiting metallic conduction; however, CRO thin films with densely connected grains exhibited high σ. The electron conduction transition from semi-conducting behavior to metallic conduction occurred when σ of 10^4 S m^{-1} was reached independent of alkaline earth metal and microstructure. The optimum conditions to prepare $ARuO_3$ thin films with higher σ were $T_{sub} = 773$ to 973 K and $P_{O_2} = 0.13$ to 13 Pa.

Acknowledgements

This research was supported in part by the Global COE Program of the Materials Integration International Center of Education and Research, Tohoku University, and by the Asian CORE Program, JSPS. This research was financially supported in part by Furuya Metal Co. Ltd. and Lonmin Plc. The authors are also grateful to Marubun Research Promotion Foundation for its financial support.

References

1. Eom, C. B., Cava, R. J., Fleming, R. M., Phillips, J. M., van Dover, R. B., Marshall, J. H. *et al.*, Single-crystal epitaxial thin films of the isotropic metallic oxides $Sr_{1-x}Ca_xRuO_3$ ($0 \le x \le 1$). *Science*, 1992, **258**, 1766–1769.
2. Fröhlich, K., Hušeková, K., Machajdík, D., Lupták, R., Ťapajna, M., Hooker, J. C. *et al.*, Preparation of $SrRuO_3$ films for advanced CMOS metal gates. *Mater. Sci. Semicond. Process.*, 2004, **7**, 265–269.
3. Randall, J. J. and Ward, R., The preparation of some ternary oxides of the platinum metals. *J. Am. Chem. Soc.*, 1959, **81**, 2629–2631.
4. Donohue, P. C., Katz, L. and Ward, R., The crystal structure of barium ruthenium oxide and related compounds. *Inorg. Chem.*, 1965, **4**, 306–310.
5. Hong, S.-T. and Sleight, A. W., Crystal structure of 4H BaRuO: high pressure phase prepared at ambient pressure. *J. Solid State Chem.*, 1997, **128**, 251–255.
6. Longo, J. M. and Kafalas, J. A., Pressure-induced structural changes in the system $Ba_{1-x}Sr_xRuO_3$. *Mater. Res. Bull.*, 1968, **3**, 687–692.
7. Miyazaki, H., Miwa, Y. and Suzuki, H., Improvement in fatigue property for a PZT ferroelectric film device with SRO electrode film prepared by chemical solution deposition. *Mater. Sci. Eng. B*, 2007, **136**, 203–206.
8. Yokoyama, S., Okamoto, S., Funakubo, H., Iijima, T., Saito, K., Okino, H. *et al.*, Crystal structure, electrical properties, and mechanical response of (1 0 0)-/(0 0 1)-oriented epitaxial $Pb(Mg_{1/3}Nb_{2/3})O_3$–$PbTiO_3$ films grown on $(100)_c SrRuO_3||(100)SrTiO_3$ substrates by metal-organic chemical vapor deposition. *J. Appl. Phys.*, 2006, **100**, 054110.
9. Char, K., Colclough, M. S., Geballe, T. H. and Myers, K. E., High T_C superconductor–normal-superconductor Josephson junctions using $CaRuO_3$ as the metallic barrier. *Appl. Phys. Lett.*, 1993, **62**, 196–198.
10. Bouchard, R. J. and Gillson, J. L., Electrical properties of $CaRuO_3$ and $SrRuO_3$ single crystals. *Mater. Res. Bull.*, 1972, **7**, 873–878.
11. Shepard, M., McCall, S., Cao, G. and Crow, J. E., Thermodynamic properties of perovskite $ARuO_3$ (A = Ca, Sr, and Ba) single crystals. *J. Appl. Phys.*, 1997, **81**, 4978–4980.
12. Fang, X. and Kobayashi, T., Characterization of $SrRuO_3$ thin film grown by laser ablation at temperatures above 400 °C. *J. Appl. Phys.*, 2001, **90**, 162–166.
13. Ito, A., Masumoto, H. and Goto, T., Microstructure and electrical conductivity of epitaxial $SrRuO_3$ thin films prepared on (0 0 1), (1 1 0) and (1 1 1) $SrTiO_3$ substrates by laser ablation. *Mater. Trans.*, 2007, **48**, 227–233.

14. Wu, X. D., Foltyn, S. R., Dye, R. C., Coulter, Y. and Muenchausen, R. E., Properties of epitaxial $SrRuO_3$ thin films. *Appl. Phys. Lett.*, 1993, **62**, 2434–2436.
15. Ito, A., Masumoto, H. and Goto, T., Effect of lattice matching on microstructure and electrical conductivity of epitaxial $ARuO_3$ (A = Sr, Ca and Ba) thin films prepared on (0 0 1) $LaAlO_3$ substrates by laser ablation. *Thin Solid Films*, 2009, **517**, 5616–5620.
16. Ito, A., Masumoto, H. and Goto, T., Microstructure and electrical conductivity of $SrRuO_3$ thin films prepared by laser ablation. *Mater. Trans.*, 2007, **47**, 2808–2814.
17. Ito, A., Masumoto, H., Goto, T. and Microstructure, Electrical conductivity of $BaRuO_3$ thin films prepared by laser ablation. *Mater. Trans.*, 2007, **48**, 2953–2959.
18. Ito, A., Masumoto, H. and Goto, T., Microstructure and electrical conductivity of $CaRuO_3$ thin films by laser ablation. *Mater. Trans.*, 2008, **49**, 158–165.
19. Keawprak, N., Tu, R. and Goto, T., Preparations of $CaRuO_3$ body by plasma sintering and its thermoelectric properties. *Mater. Trans.*, 2007, **48**, 1529–1533.
20. Ito, A., Masumoto, H. and Goto, T., Microstructure and electrical conductivity of epitaxial $CaRuO_3$ thin films prepared on (0 0 1), (1 1 0) and (1 1 1) $SrTiO_3$ substrates by laser ablation. *J. Ceram. Soc. Jpn.*, 2007, **115**, 683–687.
21. Hyun, S., Cho, J. H., Kim, A., Kim, J., Kim, T. and Char, K., Coexistence of metallic and insulating phases in epitaxial $CaRuO_3$ thin films observed by scanning microwave microscopy. *Appl. Phys. Lett.*, 2002, **80**, 1574–1576.
22. Rao, R. A., Gan, Q., Eom, C. B., Cava, R. J., Suzuki, Y., Krajewski, J. J. *et al.*, Strain stabilized metal-insulator transition in epitaxial thin films of metallic oxide $CaRuO_3$. *Appl. Phys. Lett.*, 1997, **70**, 3035–3037.
23. Sefrioui, Z., Arias, D., Navacerrada, M. A., Varela, M., Loos, G., Lucía, M. *et al.*, Metal–insulator transition in $SrRuO_3$ induced by ion irradiation. *Appl. Phys. Lett.*, 1998, **73**, 3375–3377.
24. Toyota, D., Ohkubo, I., Kumigashira, H., Oshima, M., Ohnishi, T., Lippmaa, M. *et al.*, Thickness-dependent electronic structure of ultrathin $SrRuO_3$ films studied by *in situ* photoemission spectroscopy. *Appl. Phys. Lett.*, 2005, **87**, 162508.
25. Shimizu, T. and Kawakubo, T., First-principles study on electronic structure and thermodynamic stability of $Sr(Ti,Ru)O_3$. *Jpn. J. Appl. Phys.*, 2001, **40**, L117–L119.
26. Megaw, H. D., Crystal structure of double oxides of the perovskite type. *Proc. Phys. Soc.*, 1946, **58**, 133–152.
27. Yang, H. K., Chung, J. W., Raju, G. S. R., Moona, B. K., Choi, B. C., Jeong, J. H. *et al.*, Luminescent characteristics of $CaTiO_3:Pr^{3+}$ thin films prepared by pulsed laser deposition method with various substrates. *Appl. Surf. Sci.*, 2009, **255**, 5062–5066.
28. Ito, A., Masumoto, H. and Goto, T., Effect of Ba substitution on the microstructure and electrical conductivity of $Ba_xCa_{1-x}RuO_3$ thin films prepared by laser ablation. *Mater. Trans.*, 2008, **49**, 1822–1825.